Journal of Computational Physics 228 (2009) 3540–3558

Contents lists available at ScienceDirect

Journal of Computational Physics

journal homepage: www.elsevier.com/locate/jcp

An Asymptotic Preserving scheme for the Euler equations in a strong magnetic field

P. Degond [a,b], F. Deluzet [a,b], A. Sangam [a,b,c,d,*], M.-H. Vignal [a,b]

[a] Université de Toulouse, UPS, INSA, UT1, UTM, Institut de Mathématiques de Toulouse, F-31062 Toulouse, France
[b] CNRS, Institut de Mathématiques de Toulouse UMR 5219, F-31062 Toulouse, France
[c] Université de Nice Sophia-Antipolis, Laboratoire Jean-Alexandre Dieudonné, F-06108 Nice, France
[d] CNRS, Laboratoire Jean-Alexandre Dieudonné UMR 6621, F-06108 Nice, France

ARTICLE INFO

Article history:
Received 25 July 2008
Received in revised form 1 December 2008
Accepted 25 December 2008
Available online 11 February 2009

Keywords:
Plasmas
Euler equations
Lorentz force
Large magnetic field
Drift-fluid limit
Asymptotic-Preserving scheme

ABSTRACT

This paper is concerned with the numerical approximation of the isothermal Euler equations for charged particles subject to the Lorentz force (the 'Euler–Lorentz' system). When the magnetic field is large, or equivalently, when the parameter ε representing the non-dimensional ion cyclotron frequency tends to zero, the so-called drift-fluid (or gyro-fluid) approximation is obtained. In this limit, the parallel motion relative to the magnetic field direction splits from perpendicular motion and is given implicitly by the constraint of zero total force along the magnetic field lines. In this paper, we provide a well-posed elliptic equation for the parallel velocity which in turn allows us to construct an Asymptotic-Preserving (AP) scheme for the Euler–Lorentz system. This scheme gives rise to both a consistent approximation of the Euler–Lorentz model when ε is finite and a consistent approximation of the drift limit when $\varepsilon \to 0$. Above all, it does not require any constraint on the space and time-steps related to the small value of ε. Numerical results are presented, which confirm the AP character of the scheme and its Asymptotic Stability.

1. Introduction

This paper is concerned with the construction of a numerical scheme for the system of isothermal Euler equations for charged particles subject to the Lorentz force (which we will refer to as the *Euler–Lorentz* system). More precisely, we are interested in the regime where the inertia terms which balance the pressure and Lorentz forces in the momentum balance equation are scaled by a small parameter ε. The parameter ε represents the inverse of the ion gyro-frequency around the magnetic field axis scaled by a characteristic time of the experiment. When ε tends to zero, the so-called *drift-fluid* or *gyro-fluid* regime is reached [21,27].

In the drift-fluid approximation, particles are confined along the magnetic field lines. As a consequence, the dynamics along the magnetic field lines is much quicker than across it. In the limit $\varepsilon \to 0$, the parallel motion assumes an instantaneous equilibrium in which the pressure force equilibrates the electric force. This equilibrium is attained through acoustic waves propagating at infinite velocity in a similar fashion as what happens in a low Mach number fluid. These acoustic waves adjust the parallel velocity instantaneously in such a way that this equilibrium is satisfied at all times. In this way, the parallel velocity plays the role of a Lagrange multiplier of the constraint of zero total aligned force. The first goal of this paper is

* Corresponding author. Address: Université de Nice Sophia-Antipolis, Laboratoire Jean-Alexandre Dieudonné, F-06108 Nice, France. Tel.: +33 (0)4 92 07 60 20; fax: +33 (0)4 93 51 79 74.
E-mail addresses: pierre.degond@math.univ-toulouse.fr (P. Degond), fabrice.deluzet@math.univ-toulouse.fr (F. Deluzet), afeintou.sangam@math.univ-toulouse.fr, afeintou.sangam@unice.fr (A. Sangam), marie-helene.vignal@math.univ-toulouse.fr (M.-H. Vignal).

0021-9991/$ - see front matter © 2009 Elsevier Inc. All rights reserved.
doi:10.1016/j.jcp.2008.12.040

to give an equivalent formulation of the drift-fluid approximation that enables us to calculate this parallel velocity (contrary to what is sometimes written in the literature [21], it is possible to find such an equation).

The second goal is to design a valid scheme for both regimes $\varepsilon \sim 1$ and $\varepsilon \to 0$. This scheme gives rise to both a consistent approximation of the Euler–Lorentz model when ε is finite and a consistent approximation of the drift-fluid limit when $\varepsilon \to 0$. Above all, it does not require any constraint on the space and time-steps related to the small value of ε. This type of schemes is usually referred to as *Asymptotic Preserving schemes (AP)*.

Asymptotic Preserving schemes have been proposed in a variety of contexts, such as hydrodynamic or diffusion limits of kinetic model [5,25,26,22,31,4,17], relaxation limits of hyperbolic models [23,24,18], relaxation limits of Complex-Ginzburg–Landau equations [10], low-Mach number limits of compressible fluid models [9]. In the plasma physics context, these schemes have appeared in relation with the quasineutral limit of the Euler–Poisson system [6,7,11] or Vlasov–Poisson system [8,3].

Such schemes are of great potential interest to the simulation of strongly magnetized plasmas such as those encountered in space plasmas or in Tokamak devices like ITER. First of all, there are several advantages to using the original Euler–Lorentz model instead of the limit drift-fluid model. Indeed, the drift-fluid model is a mathematically complex model: the constraint of zero total force makes it a mixed-type model, with certain characteristics of an elliptic problem, like the incompressible Navier–Stokes equation. Dealing with this constraint is numerically challenging, and is at least as difficult as dealing with the incompressibility constraint in the Navier–Stokes equation. In the literature, various drift-fluid models have been proposed on physical grounds [1,2,14–16,19,20,28–30,32,33,35]. However, their relations to the drift-fluid model which can be derived from the formal asymptotic analysis developed below are unclear. This is why we find preferable to rely on the original Euler–Lorentz model, in which the momentum conservation equation directly follows from first physical principles.

Another advantage of AP schemes is their ability to deal equally well with the asymptotic regime $\varepsilon \to 0$ and the 'normal' situation $\varepsilon = O(1)$. This is potentially very interesting for situations in which part of the simulation domain reaches the asymptotic regime and part of it does not. The usual approach for dealing with such occurrences is through multiphysics domain decomposition: the full Euler–Lorentz model is used in the region where $\varepsilon = O(1)$ and the drift-fluid limit model is used where $\varepsilon \ll 1$ (we assume the dimensionless parameter ε is computed using local estimates of the magnetic field strength and can be considered as a function of the space and time coordinates). There are several drawbacks in using this approach. The first one is the choice of the position of the interface (or cross-talk region), which can influence the outcome of the simulation. If the interface evolves in time, an algorithm for interface motion has to be devised and some adaptive remeshing has to be implemented, which requires heavy code developments and can be quite CPU time consuming. Determining the right coupling strategy between the two models can also be quite challenging and the outcome of the numerical simulations may also depend on that choice. Because these questions do not have a straightforward answer, multiphysics domain decomposition strategies often lack robustness and reliability. Here, using the original model with an AP discretization method everywhere prevents from having to introduce questionable physical artefacts in the model and permits to use the same code everywhere in both regimes.

The potential application of these methods is the simulation of fluid turbulence in Tokamak plasmas. There has been considerable literature on this problem [1,2,13,14,19,20,35]. The present work is far from being at a comparable development stage, since the present numerical tests are restricted to given uniform magnetic and electric fields in a two-dimensional setting. Nonetheless, this is an unavoidable intermediate step to check the performances of the method. The numerical tests being successful, this approach will soon be extended to an arbitrary given magnetic field and coupled to the dynamics of the electron fluid through quasineutrality assumptions.

The assumption that the ion fluid is isothermal is only made for simplicity. An energy equation for the ion fluid can be considered instead. The approach extends easily to this case. We will report on it in future work.

This paper is then organized as follows. The isothermal Euler–Lorentz model in the drift-fluid scaling and the drift-fluid limit are presented in Section 2. An Asymptotic Preserving time-discretization of the isothermal Euler–Lorentz model in the drift-fluid scaling and a full discretization of this scheme in a reduced two-dimensional setting are proposed in Section 3. Numerical results are given in Section 4 and finally, conclusions are given in Section 5.

2. The isothermal Euler–Lorentz model and the drift-fluid limit

2.1. The Euler–Lorentz model

We are concerned with the Euler–Lorentz model describing the isothermal flow of positive ions in a tokamak. In this model, we neglect the electrons and suppose that the electric and magnetic fields are given. In the *drift-fluid asymptotics*, we let ε be a typical scaled value of the gyro-period of the particles, i.e. the period of their rotation motion about the magnetic field axis. The scaled isothermal Euler–Lorentz model takes the form:

$$\partial_t n_\varepsilon + \nabla \cdot (n_\varepsilon \boldsymbol{u}_\varepsilon) = 0, \tag{2.1}$$

$$\varepsilon[\partial_t (n_\varepsilon \boldsymbol{u}_\varepsilon) + \nabla \cdot (n_\varepsilon \boldsymbol{u}_\varepsilon \otimes \boldsymbol{u}_\varepsilon)] + T \nabla n_\varepsilon = n_\varepsilon (\boldsymbol{E} + \boldsymbol{u}_\varepsilon \times \boldsymbol{B}), \tag{2.2}$$

where $n_\varepsilon, \boldsymbol{u}_\varepsilon$ are the density and the velocity of ions, respectively. The quantity T is the ion temperature. Here, the electric field $\boldsymbol{E}$ and the magnetic field $\boldsymbol{B}$ are assumed to be given functions. The symbol ∇ is the gradient operator while $\nabla\cdot$ denotes the divergent operator.

This scaled model is obtained from the unscaled Euler–Lorentz model by introducing characteristic scales for length x_0, time t_0, velocity u_0, density n_0, temperature T_0, electric field E_0 and magnetic field B_0. As usual, we set $x_0 = u_0 t_0$ and the characteristic electric and magnetic fields are assumed to follow the relation $E_0 = u_0 B_0$, so that the gyro-frequency of the ions is given by $\omega = qB_0/m = qE_0/(mu_0)$ (where q is the ion electric charge). In doing so, two dimensionless parameters appear, the Mach number $M = u_0/c_s$ where $c_s = (T_0/m)^{1/2}$ is the sound speed (and m is the ion mass) on the one hand, and the scaled gyro-period $\varepsilon = m/(qB_0 t_0)$. In the drift-fluid asymptotics, we assume that the Mach number and the gyro-period are linked by $M = \sqrt{\varepsilon}$, which leads to the scaled problem (2.1), (2.2).

The following notations will be useful: the director of the magnetic field is denoted by $\boldsymbol{b} = \boldsymbol{B}/B$ where B is the Euclidean norm of $\boldsymbol{B}$.

Any vector quantity $\boldsymbol{v}$ can be split into its *parallel* ($\|$) and *perpendicular* ($\perp$) parts as follows:

$$\boldsymbol{v} = \boldsymbol{v}_\| + \boldsymbol{v}_\perp = v_\| \boldsymbol{b} + \boldsymbol{v}_\perp, \quad v_\| = \boldsymbol{v}\cdot\boldsymbol{b}, \quad \boldsymbol{v}_\perp = \boldsymbol{b}\times(\boldsymbol{v}\times\boldsymbol{b}).$$

Next, we introduce the *parallel gradient* $\nabla_\| \phi = \boldsymbol{b}\cdot\nabla\phi$ for any scalar function ϕ. The quantity $\nabla_\|\phi$ is a scalar. In the same way, we also introduce the *parallel divergence*, given for any vector field $\boldsymbol{v}$ by $\nabla_\|\cdot(v_\|) = \nabla\cdot(v_\|\boldsymbol{b})$. This operator can be related to the parallel gradient by following equalities:

$$\nabla_\|\cdot v_\| = \nabla\cdot\left(\frac{v_\|}{B}\boldsymbol{B}\right) = B\nabla_\|\left(\frac{v_\|}{B}\right), \tag{2.3}$$

since the magnetic field is a divergence-free vector. We can write $\nabla\cdot\boldsymbol{v} = \nabla\cdot\boldsymbol{v}_\perp + \nabla_\|\cdot(v_\|)$. Note that $\nabla_\|\cdot(v_\|)$ is also a scalar. More generally, we introduce the *parallel divergence* $\nabla_\|\cdot\phi$, acting on a scalar ϕ, by $\nabla_\|\cdot\phi = \nabla\cdot(\phi\boldsymbol{b})$. The operators $\nabla_\|$ and $\nabla_\|\cdot$ are formal adjoints. Let us consider two scalar-valued functions ϕ and ψ defined on a regular domain Ω, and let us assume also that ϕ and ψ vanish on the boundary $\partial\Omega$, for simplicity. We have

$$\int_\Omega \left[\nabla_\|(\nabla_\|\cdot\phi)\right]\psi d\boldsymbol{x} = \int_\Omega [\boldsymbol{b}\cdot\nabla(\nabla\cdot(\phi\boldsymbol{b}))]\psi d\boldsymbol{x} = -\int_\Omega (\nabla\cdot(\phi\boldsymbol{b}))(\nabla\cdot(\psi\boldsymbol{b}))d\boldsymbol{x} = -\int_\Omega (\nabla_\|\cdot\phi)(\nabla_\|\cdot\psi)d\boldsymbol{x}.$$

2.2. The drift-fluid limit

The formal limit $\varepsilon\to 0$ in the isothermal Euler–Lorentz model (2.1), (2.2) leads to the so-called isothermal drift-fluid model

$$\partial_t n + \nabla\cdot(n\boldsymbol{u}) = 0, \tag{2.4}$$

$$T\nabla n = n(\boldsymbol{E} + \boldsymbol{u}\times\boldsymbol{B}). \tag{2.5}$$

The constraint (2.5) completely determines the velocity $\boldsymbol{u}$. Indeed, taking the parallel and perpendicular components of (2.5) leads to

$$n\boldsymbol{u}_\perp = \frac{1}{B}\boldsymbol{b}\times(T\nabla n - n\boldsymbol{E}), \tag{2.6}$$

$$T\nabla_\| n - nE_\| = 0. \tag{2.7}$$

After dividing by n, we find that the first term at the right-hand side of (2.6) is the diamagnetic drift velocity while the second one is the $\boldsymbol{E}\times\boldsymbol{B}$ drift velocity.

Eq. (2.7) can be recast in the form of an elliptic equation for $u_\|$. Indeed, (2.4) can be written

$$\partial_t n + \nabla_\perp\cdot(n\boldsymbol{u}_\perp) + \nabla_\|\cdot(nu_\|) = 0. \tag{2.8}$$

Applying $\nabla_\|$ to (2.8), noting that $[\nabla_\|, \partial_t] = -\partial_t b\cdot\nabla$ (where $[\cdot,\cdot]$ denotes the commutator) and inserting (2.7) leads to

$$-\nabla_\|(\nabla_\|\cdot(nu_\|)) = \partial_t\left(\frac{nE_\|}{T}\right) - \partial_t b\cdot\nabla n + \nabla_\|(\nabla_\perp\cdot(n\boldsymbol{u}_\perp)). \tag{2.9}$$

This is a one-dimensional elliptic equation for $u_\|$ along the magnetic field lines, which is well-posed through the above mentioned duality between the parallel gradient and parallel divergence operators. Therefore the parallel component $u_\|$ can be computed explicitly through the resolution of this elliptic equation, provided that adequate boundary conditions are given. The boundary conditions depend on the specific test case under consideration. They will be discussed in the numerical section below.

The drift-fluid model consists of Eqs. (2.4), (2.6) and (2.9).

Note that in general, the operator $\nabla(\nabla\cdot)$ 'gradient of divergence' is not invertible, because curls of arbitrary vector fields are non-zero elements of the kernel of this operator. However, the operator $\nabla_\|(\nabla_\|\cdot)$ involved in the drift-fluid limit (2.9) acts on the scalar $u_\|$ and is just the second derivative with respect to the one-dimensional coordinate along the magnetic field lines. Therefore, the operator $\nabla_\|(\nabla_\|\cdot)$, with suitable boundary conditions (such as Dirichlet ones) is invertible.

2.3. A reformulation of the isothermal Euler–Lorentz model

The scaled Euler–Lorentz model in the drift-fluid asymptotics (2.1), (2.2) is a singularly perturbed problem: in the drift-fluid limit (2.4), (2.5), the type of certain equations changes. Indeed, in the Euler–Lorentz model the velocity is given by a time evolution equation of hyperbolic type (2.2), while in the drift-fluid limit, the perpendicular velocity is given by an algebraic Eq. (2.6), while the parallel component is found through solving an elliptic type Eq. (2.9). Only the mass conservation equations (respectively (2.1) and (2.4)) do not change. To find an AP scheme, it is essential to 'regularize' the perturbation, i.e. to reformulate the momentum Eq. (2.2) in the Euler–Lorentz model in such a way that the limit equations for the velocity (2.6) and (2.9) appear explicitly in the system of equations. The goal of this section is to find such a reformulation.

For the perpendicular component of the momentum, we take the cross-product of (2.2) with $\boldsymbol{b}$, which leads to

$$B(n_\varepsilon \boldsymbol{u}_\varepsilon)_\perp - \varepsilon \partial_t \big(\boldsymbol{b} \times (n_\varepsilon \boldsymbol{u}_\varepsilon)_\perp\big) = -\boldsymbol{b} \times [-T\nabla n_\varepsilon + n_\varepsilon \boldsymbol{E}] + \varepsilon[-(\partial_t \boldsymbol{b}) \times (n_\varepsilon \boldsymbol{u}_\varepsilon) + \boldsymbol{b} \times (\nabla \cdot (n_\varepsilon \boldsymbol{u}_\varepsilon \otimes \boldsymbol{u}_\varepsilon))]. \tag{2.10}$$

Formally, when $\varepsilon \to 0$ in Eq. (2.10), we recover the equation for the perpendicular component of the momentum in the drift-fluid limit model (2.6).

We now take the scalar product of (2.2) with $\boldsymbol{b}$

$$\varepsilon\Big[\partial_t \Big((n_\varepsilon u_\varepsilon)_\parallel\Big) - (\partial_t \boldsymbol{b}) \cdot (n_\varepsilon \boldsymbol{u}_\varepsilon) + \boldsymbol{b} \cdot (\nabla \cdot (n_\varepsilon \boldsymbol{u}_\varepsilon \otimes \boldsymbol{u}_\varepsilon))\Big] = \boldsymbol{b} \cdot [-T\nabla n_\varepsilon + n_\varepsilon \boldsymbol{E}]. \tag{2.11}$$

Since $u_\parallel$ cannot be computed explicitly from this equation in the limit $\varepsilon \to 0$, we are led to reformulate Eq. (2.11). We first take the time derivative of (2.11) and get

$$\varepsilon\Big[\partial_t^2 \Big((n_\varepsilon u_\varepsilon)_\parallel\Big) - \partial_t((\partial_t \boldsymbol{b}) \cdot (n_\varepsilon \boldsymbol{u}_\varepsilon)) + \partial_t(\boldsymbol{b} \cdot (\nabla \cdot (n_\varepsilon \boldsymbol{u}_\varepsilon \otimes \boldsymbol{u}_\varepsilon)))\Big] = \partial_t(n_\varepsilon \boldsymbol{E}_\parallel) - T\partial_t \boldsymbol{b} \cdot \nabla n_\varepsilon - T\nabla_\parallel \partial_t n_\varepsilon. \tag{2.12}$$

Now, applying $\nabla_\parallel$ to (2.1) (rewritten in the same fashion as (2.8) leads to

$$\begin{aligned}\varepsilon\partial_t^2 \Big((n_\varepsilon u_\varepsilon)_\parallel\Big) - T\nabla_\parallel(\nabla_\parallel \cdot (n_\varepsilon u_\varepsilon)_\parallel) = {} & \varepsilon\partial_t((\partial_t \boldsymbol{b}) \cdot (n_\varepsilon \boldsymbol{u}_\varepsilon)) - \varepsilon\partial_t(\boldsymbol{b} \cdot (\nabla \cdot (n_\varepsilon \boldsymbol{u}_\varepsilon \otimes \boldsymbol{u}_\varepsilon))) + \partial_t(n_\varepsilon \boldsymbol{E}_\parallel) - T\partial_t \boldsymbol{b} \cdot \nabla n_\varepsilon \\ & + T\nabla_\parallel(\nabla_\perp \cdot (n_\varepsilon \boldsymbol{u}_\varepsilon)_\perp).\end{aligned} \tag{2.13}$$

We notice that Eq. (2.9) is the formal limit of Eq. (2.13) when $\varepsilon \to 0$. Eq. (2.13) is a wave equation for $u_\parallel$ associated with the elliptic operator $\nabla_\parallel \cdot (\nabla_\parallel)$, which is well-posed provided that suitable boundary conditions are given. This wave equation describes the propagation of disturbances along the magnetic field lines, which propagate at a velocity of order $O(\varepsilon^{-1/2})$. In the limit $\varepsilon \to 0$, an equilibrium described by (2.9) is instantaneously reached through waves propagating at infinite speed. Eq. (2.13) provides an equivalent formulation to (2.2) for $u_\parallel$, but which does not become singular when $\varepsilon \to 0$.

Therefore, the reformulation of the Euler–Lorentz model consists of Eqs. (2.1), (2.10) and (2.13).

3. An Asymptotic Preserving scheme for the isothermal Euler–Lorentz model in the drift-fluid approximation

3.1. Time semi-discrete scheme

The purpose of this section is to build an AP scheme for the Euler–Lorentz model, i.e. a scheme which is consistent with the Euler–Lorentz model when $\varepsilon = O(1)$ and with the drift-fluid limit model when $\varepsilon \ll 1$. In the present context, the AP property mostly relies on an appropriate time-discretization. We will investigate this point first. Of course, we have in mind that time semi-discrete schemes of hyperbolic problems are unstable unless some diffusion is added. In this section, we assume that the gradient operators are actually approximate operators which encompass the requested numerical diffusion. The space discretization is discussed in detail in Section 3.2.

Our AP time semi-discrete scheme relies on use of the reformulated Eqs. (2.1), (2.10) and (2.13). However, rather than looking for a discretization of them, it is more efficient to start from a discretization of the original formulation (2.1), (2.2) and find a scheme which allows the same reformulation as the continuous problem and the derivation of the discrete equivalent to (2.1), (2.10), (2.13). In this way, we are guaranteed to find a suitable discretization also in the regime $\varepsilon = O(1)$ which we could miss otherwise.

We first introduce some notations. Let $\boldsymbol{B}^m$ be the magnetic field at time t^m, B^m its magnitude and $\boldsymbol{b}^m = \boldsymbol{B}^m/B^m$ its director. For a given vector field $\boldsymbol{v}$, we denote by $(v)_\parallel^m$ and $(\boldsymbol{v})_\perp^m$ its parallel and perpendicular components with respect to $\boldsymbol{b}^m$. Similarly, we denote by $\nabla_\parallel^m$ and $\nabla_\parallel^m \cdot$ the parallel gradient and divergence operators respective to this field.

To calculate the solution of the isothermal Euler–Lorentz model in the drift-fluid approximation (2.1), (2.2), we propose the following time semi-discrete scheme:

$$\frac{n_\varepsilon^{m+1} - n_\varepsilon^m}{\Delta t} + \nabla \cdot (n_\varepsilon \boldsymbol{u}_\varepsilon)^{m+1} = 0, \tag{3.1}$$

$$\varepsilon\left[\frac{(n_\varepsilon \boldsymbol{u}_\varepsilon)^{m+1} - (n_\varepsilon \boldsymbol{u}_\varepsilon)^m}{\Delta t} + \nabla \cdot (n_\varepsilon \boldsymbol{u}_\varepsilon \otimes \boldsymbol{u}_\varepsilon)^m\right] + T(\nabla n_\varepsilon^{\#})^{m+1} = n_\varepsilon^m \boldsymbol{E}^{m+1} + (n_\varepsilon \boldsymbol{u}_\varepsilon)^{m+1} \times \boldsymbol{B}^{m+1}. \tag{3.2}$$

Here, the quantity $(\nabla n_\varepsilon^{\#})^{m+1}$ is given by

$$(\nabla n_\varepsilon^{\#})^{m+1} = (\nabla n_\varepsilon^m)_\perp^{m+1} + (\nabla n_\varepsilon^{m+1})_\parallel^{m+1} \boldsymbol{b}^{m+1}. \tag{3.3}$$

In this scheme, the mass flux, the parallel component of the pressure force and the Lorentz force are evaluated implicitly while the perpendicular component of the pressure force is evaluated explicitly. We show that these choices permit a reformulation of the scheme into discrete equivalents to Eqs. (2.1), (2.10) and (2.13).

We first investigate the transverse component and take the cross-product of (3.2) with $\boldsymbol{b}^{m+1}$. This leads to

$$(n_\varepsilon \boldsymbol{u}_\varepsilon)_\perp^{m+1} - \frac{\varepsilon}{\Delta t}\frac{1}{B^{m+1}}\boldsymbol{b}^{m+1}\times(n_\varepsilon \boldsymbol{u}_\varepsilon)_\perp^{m+1} = -\frac{1}{B^{m+1}}\boldsymbol{b}^{m+1}\times\left[\frac{\varepsilon}{\Delta t}(n_\varepsilon \boldsymbol{u}_\varepsilon)^m - \varepsilon\nabla\cdot(n_\varepsilon \boldsymbol{u}_\varepsilon\otimes\boldsymbol{u}_\varepsilon)^m - T\nabla n_\varepsilon^m + n_\varepsilon^m \boldsymbol{E}^{m+1}\right], \tag{3.4}$$

which is a discretization of Eq. (2.10), where $(\partial_t \boldsymbol{b})\times(n_\varepsilon \boldsymbol{u}_\varepsilon) \approx ((\boldsymbol{b}^{m+1}-\boldsymbol{b}^m)/\Delta t)\times(n_\varepsilon \boldsymbol{u}_\varepsilon)^m$.

We now compute the scalar product of (3.2) with $\boldsymbol{b}^{m+1}$. We get

$$\frac{\varepsilon}{\Delta t}\left((n_\varepsilon \boldsymbol{u}_\varepsilon)^{m+1}\right)_\parallel^{m+1} + T\nabla_\parallel^{m+1} n_\varepsilon^{m+1} = \boldsymbol{b}^{m+1}\cdot\left[\frac{\varepsilon}{\Delta t}(n_\varepsilon \boldsymbol{u}_\varepsilon)^m - \varepsilon\left(\nabla\cdot(n_\varepsilon \boldsymbol{u}_\varepsilon\otimes\boldsymbol{u}_\varepsilon)^m\right) + n_\varepsilon^m \boldsymbol{E}^{m+1}\right], \tag{3.5}$$

which is a discrete version of Eq. (2.11). Differentiation of the discrete mass conservation equation (3.1) in the parallel direction gives

$$\nabla_\parallel^{m+1} n_\varepsilon^{m+1} = \nabla_\parallel^{m+1} n_\varepsilon^m - \Delta t\nabla_\parallel^{m+1}\left(\nabla\cdot\left((n_\varepsilon \boldsymbol{u}_\varepsilon)^{m+1}\right)_\perp^{m+1}\right) - \Delta t\nabla_\parallel^{m+1}\left(\nabla_\parallel^{m+1}\cdot\left((n_\varepsilon u_\varepsilon)^{m+1}\right)_\parallel^{m+1}\right), \tag{3.6}$$

which can be used to eliminate n_ε^{m+1} in favor of $(n_\varepsilon u_\varepsilon)_\parallel^{m+1}$ in (3.5). This leads to

$$\begin{aligned}\frac{\varepsilon}{\Delta t}\left((n_\varepsilon \boldsymbol{u}_\varepsilon)^{m+1}\right)_\parallel^{m+1} - T\Delta t\nabla_\parallel^{m+1}\left(\nabla_\parallel^{m+1}\cdot\left((n_\varepsilon u_\varepsilon)^{m+1}\right)_\parallel^{m+1}\right) &= T\Delta t\nabla_\parallel^{m+1}\left(\nabla\cdot\left((n_\varepsilon \boldsymbol{u}_\varepsilon)^{m+1}\right)_\perp^{m+1}\right) - T\nabla_\parallel^{m+1} n_\varepsilon^m \\ &\quad + \left[\frac{\varepsilon}{\Delta t}(n_\varepsilon \boldsymbol{u}_\varepsilon)^m - \varepsilon\left(\nabla\cdot(n_\varepsilon \boldsymbol{u}_\varepsilon\otimes\boldsymbol{u}_\varepsilon)^m\right) + n_\varepsilon^m \boldsymbol{E}^{m+1}\right]_\parallel^{m+1}.\end{aligned} \tag{3.7}$$

This equation is a one-dimensional elliptic equation (along the magnetic field lines) for the quantity $((n_\varepsilon u_\varepsilon)^{m+1})_\parallel^{m+1}$. It is the discrete counterpart of (2.13) but the link with (2.13) is not fully direct. Eq. (3.7) is rather a discretization of the following equation:

$$\varepsilon\partial_t(n_\varepsilon u_\varepsilon)_\parallel - T\nabla_\parallel\left[\int_{t^m}^t \nabla_\parallel\cdot\left((n_\varepsilon u_\varepsilon)_\parallel\right)ds\right] = \varepsilon[(\partial_t \boldsymbol{b})\cdot(n_\varepsilon \boldsymbol{u}_\varepsilon) - \boldsymbol{b}\cdot(\nabla(n_\varepsilon \boldsymbol{u}_\varepsilon\otimes\boldsymbol{u}_\varepsilon))] + T\nabla_\parallel\left[\int_{t^m}^t \nabla\cdot(n_\varepsilon \boldsymbol{u}_\varepsilon)_\perp ds\right] - \boldsymbol{b}\cdot\left[T\nabla n_\varepsilon^m - n_\varepsilon \boldsymbol{E}\right], \tag{3.8}$$

which is obtained through the reformulation process outlined in Section 2.3 when the mass conservation equation is used in time-integrated form

$$n_\varepsilon = n_\varepsilon^m - \int_{t^m}^t \nabla\cdot\left((n_\varepsilon \boldsymbol{u}_\varepsilon)_\perp\right)ds - \int_{t^m}^t \nabla_\parallel\cdot\left((n_\varepsilon u_\varepsilon)_\parallel\right)ds. \tag{3.9}$$

That (3.8) is equivalent to (2.13) is easy and is left to the reader.

Now, we investigate the limit $\varepsilon\to 0$ in (3.4, 3.7), leaving Δt unchanged. We get

$$(n\boldsymbol{u})_\perp^{m+1} = -\frac{1}{B^{m+1}}\boldsymbol{b}^{m+1}\times\left[-T\nabla n^m + n^m \boldsymbol{E}^{m+1}\right], \tag{3.10}$$

$$-T\Delta t\nabla_\parallel^{m+1}\left(\nabla_\parallel^{m+1}\cdot\left((nu)^{m+1}\right)_\parallel^{m+1}\right) = T\Delta t\nabla_\parallel^{m+1}\left(\nabla\cdot\left((n\boldsymbol{u})^{m+1}\right)_\perp^{m+1}\right) - T\nabla_\parallel^{m+1} n^m + [n^m \boldsymbol{E}^{m+1}]_\parallel^{m+1}. \tag{3.11}$$

This is the discrete counterpart of the drift-fluid equations (2.6), (2.9). Therefore, the limit $\varepsilon\to 0$ can be taken in the scheme (3.1), (3.4), (3.7) and the resulting scheme is consistent with the drift-fluid equations. This shows that the time semi-discrete scheme (3.1), (3.4), (3.7) provides an Asymptotic Preserving discretization of the Euler–Lorentz model in the drift-fluid limit. This scheme enables us to compute the solution of the isothermal Euler–Lorentz model for all regimes ranging from $\varepsilon = O(1)$ to $\varepsilon \ll 1$ with the same time-step Δt. A conventional scheme would require to let $\Delta t\to 0$ simultaneously with $\varepsilon\to 0$. An AP scheme is free from this constraint.

As a comparison, let us investigate the conventional time semi-discrete scheme for the Euler–Lorentz model and show that it cannot be uniformly stable with respect to ε and cannot be AP. The conventional time semi-discrete scheme for the Euler–Lorentz model is the following:

$$\frac{n_\varepsilon^{m+1} - n_\varepsilon^m}{\Delta t} + \nabla\cdot(n_\varepsilon \boldsymbol{u}_\varepsilon)^m = 0, \tag{3.12}$$

$$\varepsilon\left[\frac{(n_\varepsilon \boldsymbol{u}_\varepsilon)^{m+1} - (n_\varepsilon \boldsymbol{u}_\varepsilon)^m}{\Delta t} + \nabla\cdot(n_\varepsilon \boldsymbol{u}_\varepsilon\otimes\boldsymbol{u}_\varepsilon)^m\right] + T\nabla n_\varepsilon^m = n_\varepsilon^{m+1}\boldsymbol{E}^{m+1} + (n_\varepsilon \boldsymbol{u}_\varepsilon)^{m+1}\times\boldsymbol{B}^{m+1}. \tag{3.13}$$

The difference with our scheme is that the mass flux and the pressure force are both evaluated explicitly. We note that the Lorentz force at the right-hand side of (3.13) is still implicit otherwise some obvious instabilities arise in the discretization of the cyclotron rotation (the $\boldsymbol{u}\times\boldsymbol{B}$ term in the Lorentz force). The hyperbolic part of this scheme has obviously a stability constraint of the form $\Delta t/\sqrt{\varepsilon}=O(1)$ and can be neither uniformly stable, nor AP. In Section 4.3, simulations are carried out which confirm that this conventional time semi-discrete scheme is not AP.

We also see that in our AP scheme, we need to evaluate both the mass flux and the parallel component of the pressure force to get an elliptic equation for $(nu)_\parallel$. If the pressure force alone is taken implicitly, this results in an equation for $(nu)_\parallel$ which is ill-posed.

3.2. Fully discrete scheme

3.2.1. A two-dimensional case

For the sake of simplicity, we restrict ourselves to a two-dimensional case with a constant in time, uniform in space magnetic field lying in the computational plane. Therefore, we assume that the magnetic field is directed along the y-axis and that the plasma lies in x,y-plane, with translation invariance in the z-direction. However, a possible non-zero plasma velocity is assumed in the z direction. In these conditions, the isothermal Euler–Lorentz model in the drift-fluid asymptotics (2.1), (2.2) is written (we now omit the indices ε for the sake of simplicity),

$$\begin{aligned}
&\partial_t n+\partial_x(nu_x)+\partial_y(nu_y)=0,\\
&\varepsilon\left[\partial_t(nu_x)+\partial_x(nu_x^2)+\partial_y(nu_xu_y)\right]+T\partial_x n=nE_x-nu_zB_y,\\
&\varepsilon\left[\partial_t(nu_y)+\partial_x(nu_xu_y)+\partial_y(nu_y^2)\right]+T\partial_y n=nE_y,\\
&\varepsilon\left[\partial_t(nu_z)+\partial_x(nu_xu_z)+\partial_y(nu_yu_z)\right]=nE_z+nu_xB_y,
\end{aligned}\tag{3.14}$$

Then the time semi-discrete AP scheme for the system (3.14) reads

$$\frac{n^{m+1}-n^m}{\Delta t}+\partial_x(nu_x)^{m+1}+\partial_y(nu_y)^{m+1}=0,\tag{3.15}$$

$$(nu_x)^{m+1}-\frac{\varepsilon}{\Delta t}\frac{1}{B}(nu_z)^{m+1}=-\frac{1}{B}\left[\frac{\varepsilon}{\Delta t}(nu_z)^m-\varepsilon\left(\partial_x(nu_xu_z)^m+\partial_y(nu_yu_z)^m\right)+n^mE_z\right],\tag{3.16}$$

$$\frac{\varepsilon}{\Delta t}\frac{1}{B}(nu_x)^{m+1}+(nu_z)^{m+1}=-\frac{1}{B}\left[-\frac{\varepsilon}{\Delta t}(nu_x)^m+\varepsilon\left(\partial_x(nu_x^2)^m+\partial_y(nu_xu_y)^m\right)+T\partial_x n^m-n^mE_x\right],\tag{3.17}$$

$$\frac{\varepsilon}{\Delta t}(nu_y)^{m+1}-T\Delta t\partial_y\left(\partial_y(nu_y)^{m+1}\right)=T\Delta t\partial_y\left(\partial_x(nu_x)^{m+1}\right)+\left[\frac{\varepsilon}{\Delta t}(nu_y)^m-\varepsilon\left(\partial_x(nu_xu_y)^m+\partial_y(nu_y^2)^m\right)-T\partial_y n^m\right]+n^mE_y,\tag{3.18}$$

where $B=\boldsymbol{b}\cdot\boldsymbol{B}=B_y$. We now give the full space-time discretization based on the above discussed AP scheme for system (3.14).

3.2.2. Fully discrete scheme in the two-dimensional case

For numerical purpose, let us consider a Cartesian mesh of the calculation domain $(x_{i-1/2},x_{i+1/2})\times(y_{j-1/2},y_{j+1/2})$, $i,j=1,\ldots,N$. Then Eqs. (3.16)–(3.18) and (3.15) are discretized according to

$$\begin{aligned}
&(nu_x)_{ij}^{m+1}-\frac{\varepsilon}{\Delta t}\frac{1}{B}(nu_z)_{ij}^{m+1}\\
&\quad=-\frac{1}{B}\left[\frac{\varepsilon}{\Delta t}(nu_z)_{ij}^m-\frac{\varepsilon}{\Delta x}\left((nu_xu_z)_{i+1/2j}^m-(nu_xu_z)_{i-1/2j}^m\right)+\frac{\varepsilon}{\Delta y}\left((nu_yu_z)_{ij+1/2}^m-(nu_yu_z)_{ij-1/2}^m\right)+(n^mE_z)_{ij}\right],
\end{aligned}\tag{3.19}$$

$$\begin{aligned}
&\frac{\varepsilon}{\Delta t}\frac{1}{B}(nu_z)_{ij}^{m+1}+(nu_x)_{ij}^{m+1}\\
&\quad-\frac{1}{B}\left[-\frac{\varepsilon}{\Delta t}(nu_x)_{ij}^m+\frac{\varepsilon}{\Delta x}\left(\left(nu_x^2+\frac{T}{\varepsilon}n\right)_{i+1/2j}^m-\left(nu_x^2+\frac{T}{\varepsilon}n\right)_{i-1/2j}^m\right)+\frac{\varepsilon}{\Delta y}\left((nu_xu_y)_{ij+1/2}^m-(nu_xu_y)_{ij-1/2}^m\right)-(n^mE_x)_{ij}\right],
\end{aligned}\tag{3.20}$$

$$\begin{aligned}
&\frac{\varepsilon}{\Delta t}(nu_y)_{ij}^{m+1}-T\Delta t(\partial_y^2(nu_y)^{m+1})_{ij}=T\Delta t\left(\partial_y(\partial_x(nu_x)^{m+1})\right)_{ij}\\
&\quad+\left[\frac{\varepsilon}{\Delta t}(nu_y)_{ij}^m-\frac{\varepsilon}{\Delta x}\left((nu_xu_y)_{i+1/2j}^m-(nu_xu_y)_{i-1/2j}^m\right)-\frac{\varepsilon}{\Delta y}\left(\left(nu_y^2+\frac{T}{\varepsilon}n\right)_{ij+1/2}^m-\left(nu_y^2+\frac{T}{\varepsilon}n\right)_{ij-1/2}^m\right)\right]+(nE_y)_{ij}^{m+1},
\end{aligned}\tag{3.21}$$

$$\frac{n_{ij}^{m+1}-n_{ij}^m}{\Delta t}+\frac{1}{\Delta x}\left((nu_x)_{i+1/2j}^{m+1}-(nu_x)_{i-1/2j}^{m+1}\right)+\frac{1}{\Delta y}\left((nu_y)_{ij+1/2}^{m+1}-(nu_y)_{ij-1/2}^{m+1}\right)=0.\tag{3.22}$$

Here n_{ij}^{m+1} is the density in the cell $(x_{i-1/2}, x_{i+1/2}) \times (y_{j-1/2}, y_{j+1/2})$ at the time t^{m+1}. The quantity $((nu_x)_{ij}^{m+1}, (nu_z)_{ij}^{m+1})^t$ is the perpendicular part of the momentum while $(nu_y)_{ij}^{m+1}$ is the parallel part of the momentum in the cell $(x_{i-1/2}, x_{i+1/2}) \times (y_{j-1/2}, y_{j+1/2})$ at the time t^{m+1}. The terms $(\cdot)_{i+1/2j}$ and $(\cdot)_{ij+1/2}$ denote the numerical fluxes at the interfaces $x_{i+1/2}$ and $y_{j+1/2}$ of the corresponding quantities, respectively. The second order terms $(\partial_y^2 (nu_y)^{m+1})_{ij}$ and $(\partial_y(\partial_x (nu_x)^{m+1}))_{ij}$ will be discussed below.

3.2.3. Discretization of the hyperbolic part

To calculate the numerical fluxes at the interfaces $(\cdot)_{i+1/2j}$ and $(\cdot)_{ij+1/2}$, we use the P_0 scheme [12]. To be more precise, let us consider the interface $x_{i+1/2}$ separating data $\mathcal{U}_{ij}^m, \mathcal{U}_{i+1j}^m$ for the corresponding Riemann problem at time t^m, where

$$\mathcal{U}_{ij}^m = (n_{ij}^m, (n\boldsymbol{u})_{ij}^m)^t, \mathcal{U}_{i+1j}^m = (n_{i+1j}^m, (n\boldsymbol{u})_{i+1j}^m)^t.$$

Let us denote by $\widehat{\mathcal{U}}_{i+1/2j}^m = (\hat{n}_{i+1/2j}^m, \widehat{n\boldsymbol{u}}_{i+1/2j}^m)^t$ the average state between the states $\mathcal{U}_{ij}^m, \mathcal{U}_{i+1j}^m$. The average state $\widehat{\mathcal{U}}_{i+1/2j}^m$ is the Roe average state [34] given here by following formula:

$$\hat{n}_{i+1/2j}^m = \sqrt{n_{ij}^m n_{i+1j}^m},$$

$$\hat{\boldsymbol{u}}_{i+1/2j}^m = \frac{\sqrt{n_{ij}^m}\boldsymbol{u}_{ij}^m + \sqrt{n_{i+1j}^m}\boldsymbol{u}_{i+1j}^m}{\sqrt{n_{ij}^m} + \sqrt{n_{i+1j}^m}}$$

and the momentum of the average state is reconstructed as

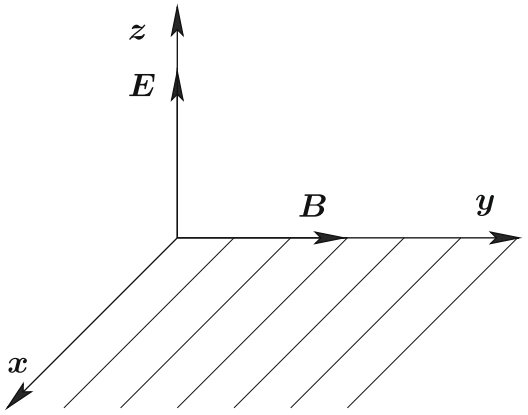

Fig. 1. The test-case geometry.

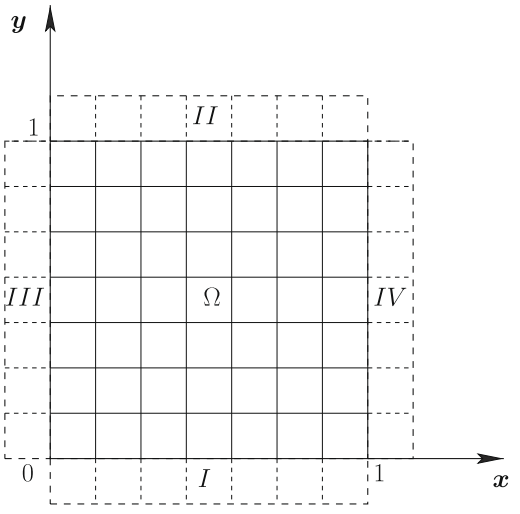

Fig. 2. Schematics of the computational domain.

$\widehat{n\boldsymbol{u}}^m_{i+1/2j} = \hat{n}^m_{i+1/2j}\hat{\boldsymbol{u}}^m_{i+1/2j}$.

Then the numerical fluxes are given by

$$(nu_xu_z)^m_{i+1/2j} = \frac{(nu_xu_z)^m_{ij} + (nu_xu_z)^m_{i+1j}}{2} - \frac{a^m_{i+1/2j}}{2}\Big((nu_z)^m_{i+1j} - (nu_z)^m_{ij}\Big), \tag{3.23}$$

$$\left(nu_x^2 + \frac{T}{\varepsilon}n\right)^m_{i+1/2j} = \frac{(nu_x^2 + \frac{T}{\varepsilon}n)^m_{ij} + (nu_x^2 + \frac{T}{\varepsilon}n)^m_{i+1j}}{2} - \frac{a^m_{i+1/2j}}{2}\Big((nu_x)^m_{i+1j} - (nu_x)^m_{ij}\Big), \tag{3.24}$$

$$(nu_xu_y)^m_{i+1/2j} = \frac{(nu_xu_y)^m_{ij} + (nu_xu_y)^m_{i+1j}}{2} - \frac{a^m_{i+1/2j}}{2}\Big((nu_y)^m_{i+1j} - (nu_y)^m_{ij}\Big), \tag{3.25}$$

$$(nu_x)^{m+1}_{i+1/2j} = \frac{(nu_x)^{m+1}_{ij} + (nu_x)^{m+1}_{i+1j}}{2} - \frac{a^m_{i+1/2j}}{2}(n^m_{i+1j} - n^m_{ij}), \tag{3.26}$$

$$(nu_y)^{m+1}_{i+1/2j} = \frac{(nu_y)^{m+1}_{ij} + (nu_y)^{m+1}_{i+1j}}{2} - \frac{a^m_{i+1/2j}}{2}(n^m_{i+1j} - n^m_{ij}). \tag{3.27}$$

Here, the speed $a^m_{i+1/2j}$ is given by

Table 1
Simulation parameters for the test-case.

	Ω	I	II	III	IV
n	1	$1+\varepsilon$	1	$1+\varepsilon$	1
nu_x	0	-1	-1	$-1+\varepsilon$	$-1+\varepsilon$
nu_y	0	1	$1+\varepsilon$	$1+\varepsilon$	1
nu_z	0	0	ε	0	ε
T	1	1	1	1	1
B_y	1	1	1	1	1
E_z	1	1	1	1	1

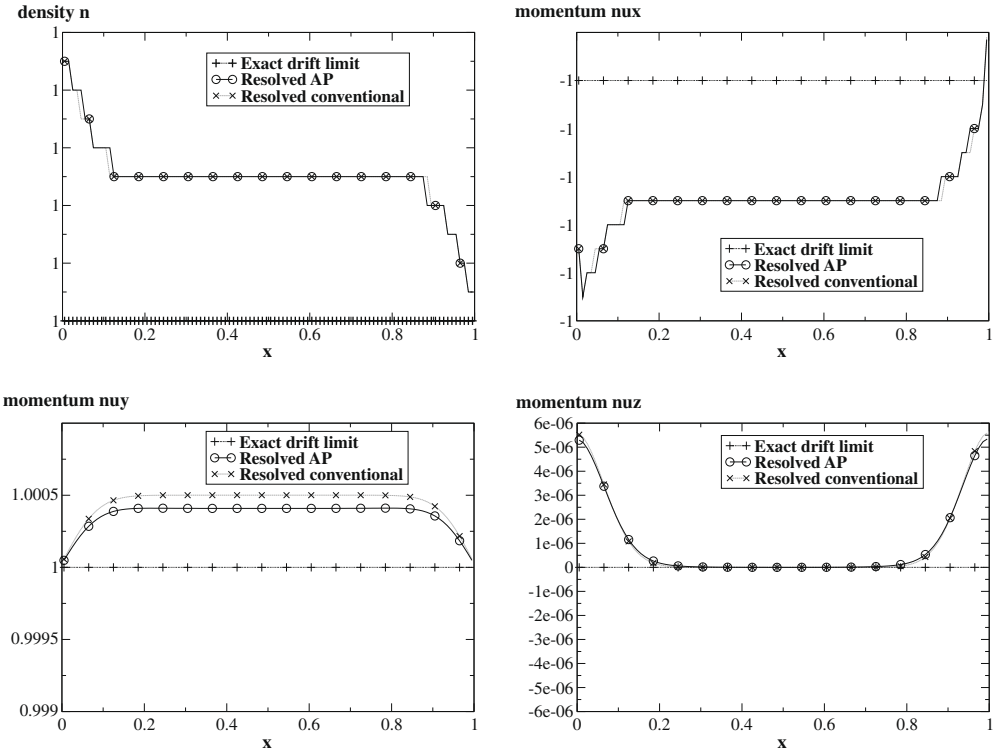

Fig. 3. Comparison of the resolved conventional scheme (crosses), the resolved AP scheme (circles) and the exact drift-fluid limit (vertical bars) at $t = 0.1$ for $\varepsilon = 10^{-6}$; density n (top left), x-component of the momentum nu_x (top right), y-component of the momentum nu_y (bottom left), z-component of the momentum nu_z (bottom right).

$$a^m_{i+1/2j} = \max(|a^{m,-}_{i+1/2j}|, |a^{m,+}_{i+1/2j}|). \tag{3.28}$$

with

$$\begin{aligned} a^{m,-}_{i+1/2j} &= \min(u^m_{xij} - c^\varepsilon, \hat{u}^m_{x_i+1/2j} - c^\varepsilon), \\ a^{m,+}_{i+1/2j} &= \max(\hat{u}^m_{x_i+1/2j} + c^\varepsilon, u^m_{x_i+1j} + c^\varepsilon) \end{aligned} \tag{3.29}$$

and $c^\varepsilon = \sqrt{T/\varepsilon}$ standing for the sound speed. The numerical fluxes across interfaces $y_{j+1/2}$ are computed similarly.

3.2.4. Discretization of the second order terms

The second order terms are computed with centered spatial discretizations

$$(\partial^2_y (nu_y)^{m+1})_{ij} = \frac{(nu_y)^{m+1}_{ij+1} - 2(nu_y)^{m+1}_{ij} + (nu_y)^{m+1}_{ij-1}}{\Delta y^2}$$

and

$$(\partial_y(\partial_x(nu_x)^{m+1}))_{ij} = \frac{1}{\Delta y}\left[(\partial_x(nu_x)^{m+1})_{ij+1/2} - (\partial_x(nu_x)^{m+1})_{ij-1/2}\right],$$

where

$$(\partial_x(nu_y)^{m+1})_{ij+1/2} = \frac{1}{2}(\partial_x(nu_x)^{m+1})_{ij+1} + \frac{1}{2}(\partial_x(nu_x)^{m+1})_{ij} = \frac{1}{2}\frac{(nu_x)^{m+1}_{i+1j+1} - (nu_x)^{m+1}_{i-1j+1}}{2\Delta x} + \frac{1}{2}\frac{(nu_x)^{m+1}_{i+1j} - (nu_x)^{m+1}_{i-1j}}{2\Delta x}.$$

To solve the elliptic equation for (nu_y), suitable boundary conditions need to be specified. In particular, using above discretizations Eq. (3.21) can be recast in the form

$$\mathcal{A}\mathcal{X}^{m+1} = \mathcal{R}\mathcal{H}\mathcal{S}^{m+1}, \tag{3.30}$$

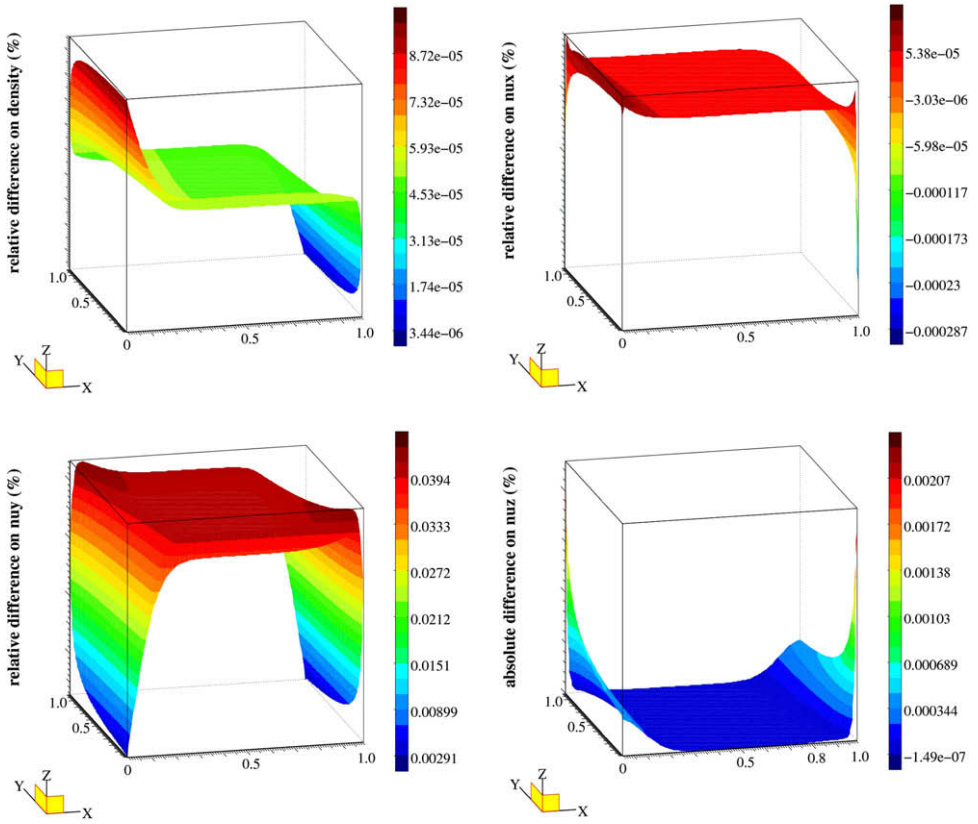

Fig. 4. Relative difference between the computed solution and the exact drift-fluid limit of the resolved AP scheme at time $t = 0.1$ for $\varepsilon = 10^{-6}$; density n (top left), x-component of the momentum nu_x (top right), y-component of the momentum nu_y (bottom left). Absolute difference between the computed solution and the exact drift-fluid limit on the z-component of the momentum nu_z (bottom right).

where $\mathcal{A} = \mathcal{A}(\varepsilon, \Delta t, \Delta y, T)$ is a regular matrix, $\mathcal{X}^{m+1} = ((nu_y)_{ij}^{m+1})_{i,j=1..N}$ is the vector of the parallel momenta in all the computational domain and $\mathcal{RHS}^{m+1} = \mathcal{RHS}^{m+1}(\varepsilon, \Delta t, \Delta x, \Delta y, T, (nu_x)^m, (nu_y)^m, E_y^m)$ is the right-hand side, which is known. The linear system (3.30) is solved by a Gaussian elimination method with partial pivoting.

3.2.5. Choice of the time-step

As usual, the time-step Δt is chosen such that the CFL condition is satisfied. In 2D geometry, this condition takes the following form:

Table 2
Maximum of relative difference between the computed solution and the exact drift-fluid limit (%) from the resolved conventional scheme on the density n, x-component of the momentum nu_x, y-component of the momentum nu_y and absolute difference between the computed solution and the exact drift-fluid limit on the z-component of the momentum nu_z.

ε	n	nu_x	nu_y	nu_z
10^{-5}	0.0087	0.00714	0.145	0.0174
10^{-6}	8.68×10^{-5}	0.000274	0.0455	0.00204
1.5×10^{-8}	1.29×10^{-6}	1.25×10^{-6}	0.00554	3.11×10^{-5}

Table 3
Maximum of relative difference between the computed solution and the exact drift-fluid limit (%) from the resolved AP scheme on the density n, x-component of the momentum nu_x, y-component of the momentum nu_y, and maximum of absolute difference between the computed solution and the exact drift-fluid limit on the z-component of the momentum nu_z.

ε	n	nu_x	nu_y	nu_z
10^{-5}	0.00873	0.0074	0.126	0.017
10^{-6}	8.72×10^{-5}	0.000287	0.0394	0.00207
1.5×10^{-8}	1.3×10^{-6}	1.25×10^{-6}	0.0048	3.16×10^{-5}

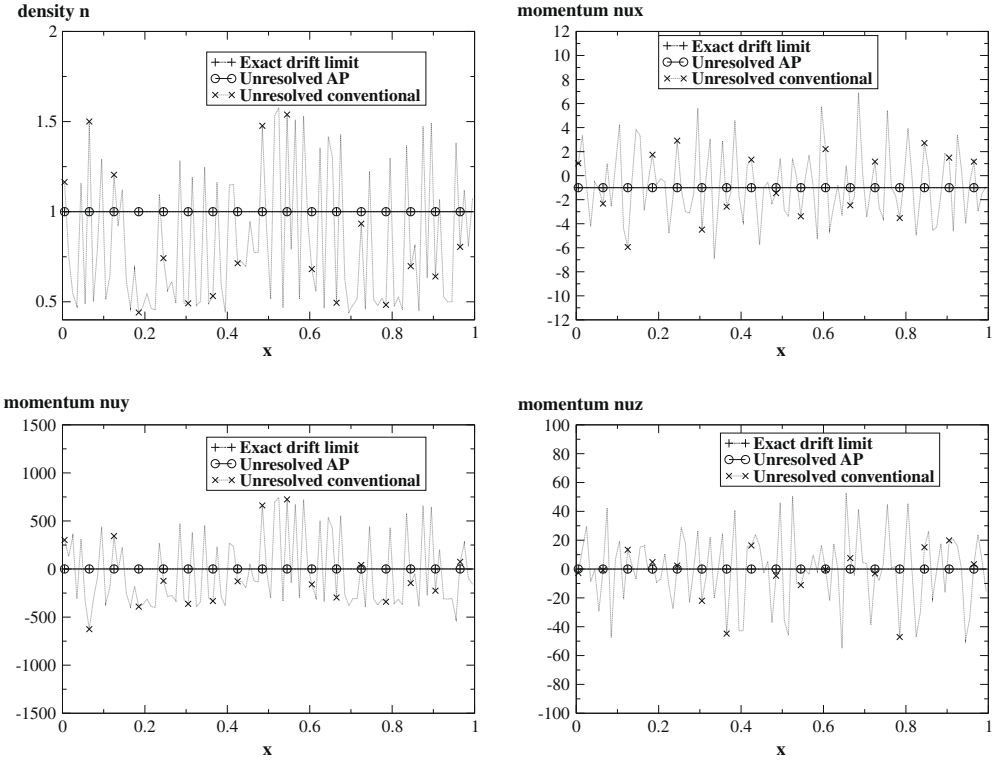

Fig. 5. Comparison of the non-resolved conventional scheme (crosses), the non-resolved AP scheme (circles) and the exact drift-fluid limit (vertical bars) at $t = 0.1$ for $\varepsilon = 10^{-6}$; density n (top left), x-component of the momentum nu_x (top right), y-component of the momentum nu_y (bottom left), z-component of the momentum nu_z (bottom right).

$$\Delta t\left(\frac{1}{\Delta x}\max_{1\leqslant i,j\leqslant N} a^m_{i+1/2j}+\frac{1}{\Delta y}\max_{1\leqslant i,j\leqslant N} a^m_{ij+1/2}\right)=CFL\leqslant 1, \tag{3.31}$$

where $a^m_{i+1/2j}$ is defined by (3.28). The scheme (3.19)–(3.21) and (3.22) with the time-step algorithm (3.31) will be referred to as the *resolved AP scheme*.

When ε tends to 0, the sound speed $c^\varepsilon=\sqrt{T/\varepsilon}$ takes large values and the time-step calculated from (3.31) becomes very small. Due to the AP character of the scheme, we do not need to constrain the time-step to stay of the order of $\sqrt{\varepsilon}$. Therefore, the sound speed can be removed from the definition of the velocities used to compute the numerical viscosity in the interfacial fluxes. These new velocities are defined as follows:

$$\tilde a^m_{i+1/2j}=\max\left(|\tilde a^{m,-}_{i+1/2j}|,|\tilde a^{m,+}_{i+1/2j}|\right) \tag{3.32}$$

with

$$\tilde a^{m,-}_{i+1/2j}=\min(u^m_{xij},\hat u^m_{x_i+1/2j}),\quad \tilde a^{m,+}_{i+1/2j}=\max(\hat u^m_{x_i+1/2j},u^m_{x_i+1j}) \tag{3.33}$$

and a new CFL condition is introduced

$$\Delta t\left(\frac{1}{\Delta x}\max_{1\leqslant i,j\leqslant N} \tilde a^m_{i+1/2j}+\frac{1}{\Delta y}\max_{1\leqslant i,j\leqslant N} \tilde a^m_{ij+1/2}\right)=CFL\leqslant 1. \tag{3.34}$$

It is important to notice that, with this new expression, the time-step can be chosen independent of ε.

The scheme (3.19)–(3.21) and (3.22) where velocities $a^m_{i+1/2j}$ are substituted by $\tilde a^m_{i+1/2j}$ given by Eq. (3.33) and with the time-step algorithm (3.34) will be called the *non-resolved AP scheme*. The numerical tests will show that this choice gives rise to a correct solution.

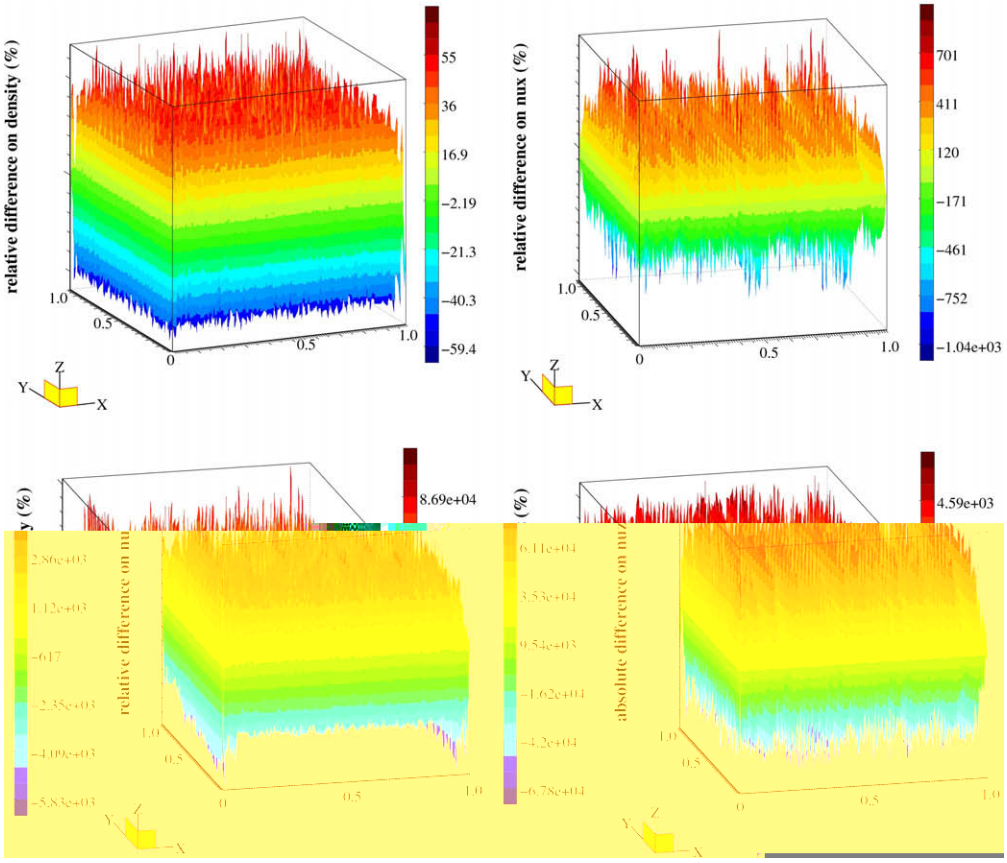

Fig. 6. Relative difference between the computed solution and the exact drift-fluid limit of the non-resolved conventional scheme at time $t=0.1$ for $\varepsilon=10^{-6}$; density n (top left), x-component of the momentum nu_x (top right), y-component of the momentum nu_y (bottom left). Absolute difference between the computed solution and the exact drift-fluid limit on the z-component of the momentum nu_z (bottom right).

4. Numerical tests

4.1. Geometry and test case

Our test-case is two-dimensional: the physical quantities depend only on the coordinates x, y. The magnetic field is assumed to be uniform and directed along the y-axis, i.e. $\boldsymbol{B} = (0, B_y, 0)$ while the electric field is directed along the z-axis, $\boldsymbol{E} = (0, 0, E_z)$. The test-case geometry is depicted in Fig. 1.

The domain is a square of side 1 as shown in Fig. 2 while the parameters are given in the Table 1: the initial values of physical quantities are put in the Ω column while the boundary conditions are given in the columns I, II, III and IV, accordingly.

For the considered test case, the exact drift-fluid approximation is stationary and uniform in the whole domain, and given by

$$n = 1, \quad nu_x = -1, \quad nu_y = 1, \quad nu_z = 0, \quad T = 1. \tag{4.1}$$

We observe that the initial and boundary data are'well prepared': they are perturbations of order ε of the drift-fluid limit. Indeed, if 'unprepared' initial and boundary data are used, large (of order 1) initial and boundary layers appear in which the exact solution is significantly different from the drift-fluid limit. In order to correctly capture these initial or boundary layers, there is no other way than using a time and space resolved scheme in which both the time and space steps are of order ε. However, the goal of an AP scheme is **not** to capture the initial and boundary layers accurately, but to provide a consistent approximation of the correct drift-fluid limit where it applies, i.e. away from these layers. An accurate verification of this property requires a test solution which is not polluted by the initial and boundary layers and therefore, the need of well-prepared initial and boundary conditions. In Section 4.4, for the sake of completeness, we show some numerical results with unprepared initial and boundary conditions.

4.2. Simulations for $\varepsilon \ll 1$

Here we would like to demonstrate that the AP scheme is consistent with the drift-fluid limit even for large time-steps compared to ε. By contrast, the conventional scheme is shown to be unstable for time-steps larger than ε. Three values of the

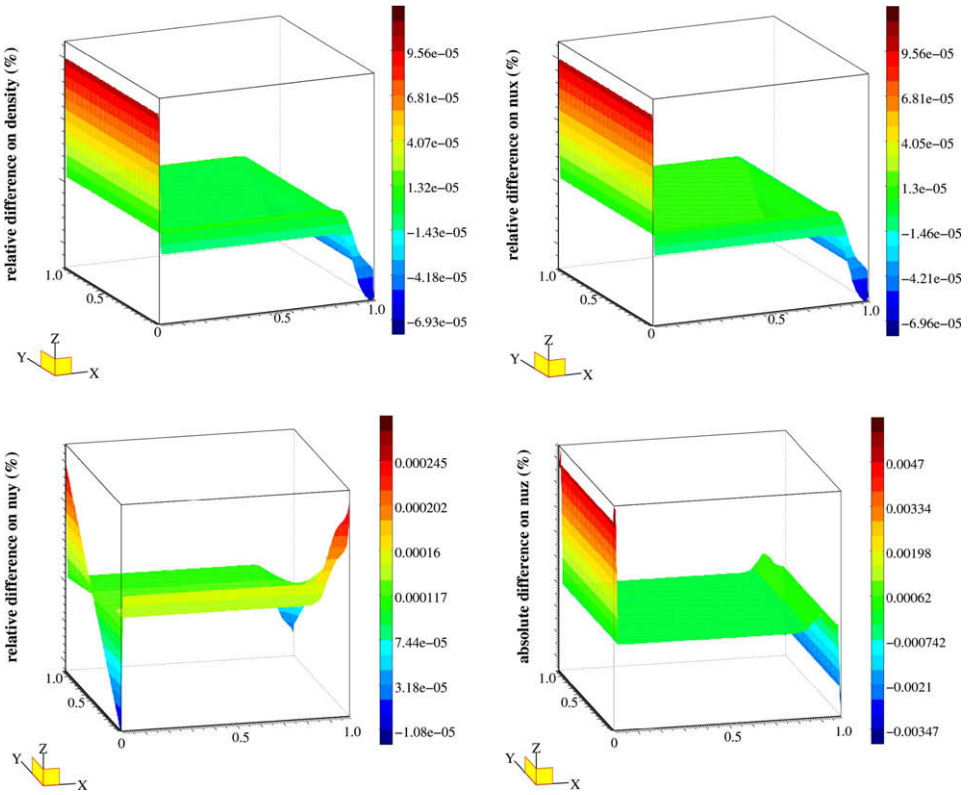

Fig. 7. Relative difference between the computed solution and the exact drift-fluid limit of the non-resolved AP scheme at time $t = 0.1$ for $\varepsilon = 10^{-6}$; density n (top left), x-component of the momentum nu_x (top right), y-component of the momentum nu_y (bottom left). Absolute difference between the computed solution and the exact drift-fluid limit on the z-component of the momentum nu_z (bottom right).

parameter ε are used: $\varepsilon = 10^{-5}$, $\varepsilon = 10^{-6}$ and $\varepsilon = \sqrt{\varepsilon_{machine}} = 1.510^{-8}$. For these values, we observe the numerical solution at times 1, 0.1 and 0.01, respectively. The reason for choosing smaller observation times when ε is smaller is due to the increase of computation time when the time-step resolves ε. The CFL number is taken equal to 0.5 for all simulations. A uniform mesh is used for both the x and y direction with steps $\Delta x = \Delta y = 0.01$.

4.2.1. Resolved case

We first compare the conventional and AP schemes in the resolved case, i.e. when Δt is smaller than ε. The results given by both the conventional and AP schemes are displayed in Fig. 3 for $\varepsilon = 10^{-6}$ and compared with the drift-fluid limit. Here, as

Table 4
Maximum of relative difference between the computed solution and the exact drift-fluid limit (%) from the non-resolved conventional scheme on the density n, x-component of the momentum nu_x, y-component of the momentum nu_y and maximum of absolute difference between the computed solution and the exact drift-fluid limit on the z-component of the momentum nu_z.

ε	n	nu_x	nu_y	nu_z
10^{-5}	75.2	1.98×10^3	2.57×10^3	6.58×10^3
10^{-6}	59.4	1.04×10^3	8.69×10^4	5.83×10^3
1.5×10^{-8}	58	118	6.44×10^5	4.64×10^3

Table 5
Maximum of relative difference between the computed solution and the exact drift-fluid limit (%) from the non-resolved AP scheme on the density n, x-component of the momentum nu_x, y-component of the momentum nu_y, and maximum of absolute difference between the computed solution and the exact drift-fluid limit on the z-component of the momentum nu_z.

ε	n	nu_x	nu_y	nu_z
10^{-5}	0.00104	0.00104	0.00255	0.0447
10^{-6}	9.56×10^{-5}	6.96×10^{-5}	0.000245	0.0047
1.5×10^{-8}	2.75×10^{-6}	7.12×10^{-6}	0.000554	0.00389

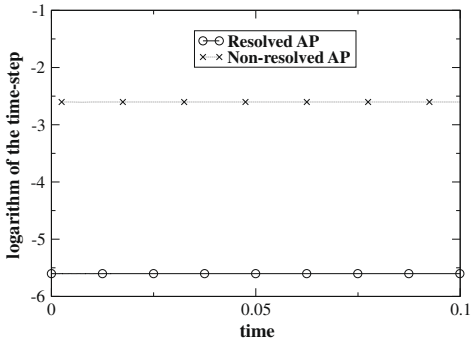

Fig. 8. Time-step (log scale) as a function of time for the resolved and non-resolved AP schemes when $\varepsilon = 10^{-6}$.

Table 6
Logarithms of the gyro-period τ, maximum of time-steps used in the resolved AP scheme (AP) and non-resolved AP scheme (NAP).

ε	τ	AP	NAP
10^{-5}	−5	−5.09	−2.6
10^{-6}	−6	−5.6	−2.6
1.5×10^{-8}	−7.83	−6.51	−2.6

Table 7
CPU time (in s) used in the resolved conventional scheme (CONV) and non-resolved AP scheme (NAP) for computing the Euler–Lorentz model at final time t_{fin} (in s). Ratio of the CPU time of the conventional to the non-resolved AP schemes.

ε	t_{fin}	CONV	NAP	CONV/NAP
10^{-5}	1.00	4940.32	13.84	357
10^{-6}	0.1	1584.21	1.39	1140
1.510^{-8}	0.01	1149.54	0.17	6762

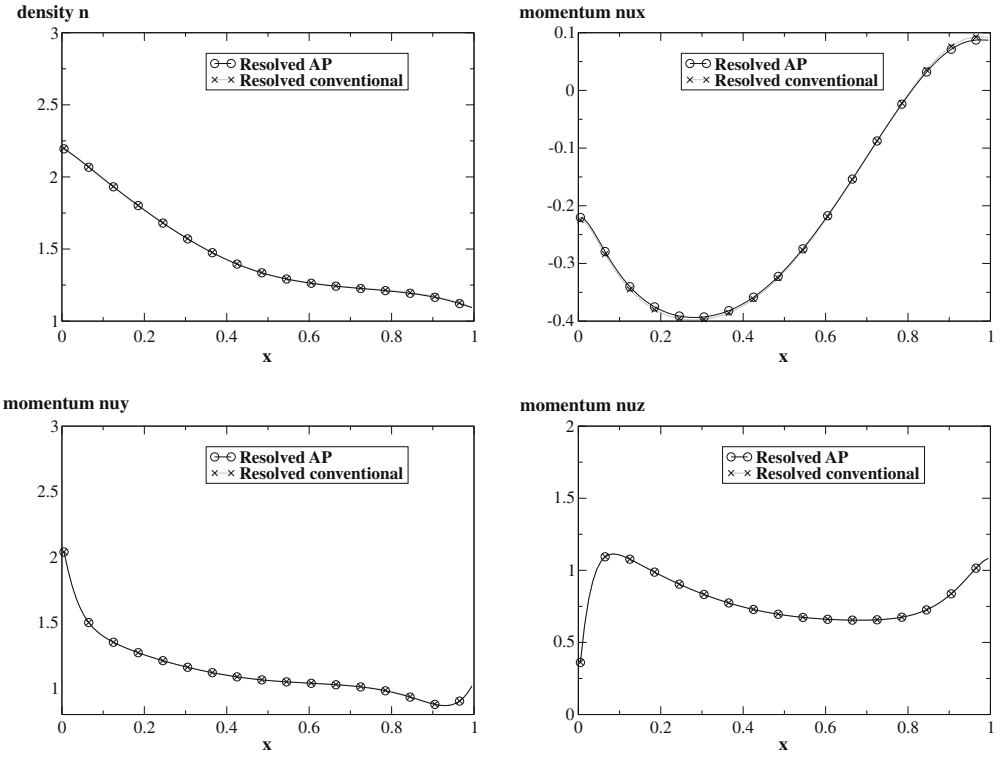

Fig. 9. Comparison of the conventional scheme (crosses), and resolved AP scheme (circles) at $t = 1$ for $\varepsilon = 1$; density n (top left), x-component of the momentum nu_x (top right), y-component of the momentum nu_y (bottom left), z-component of the momentum nu_z (bottom right).

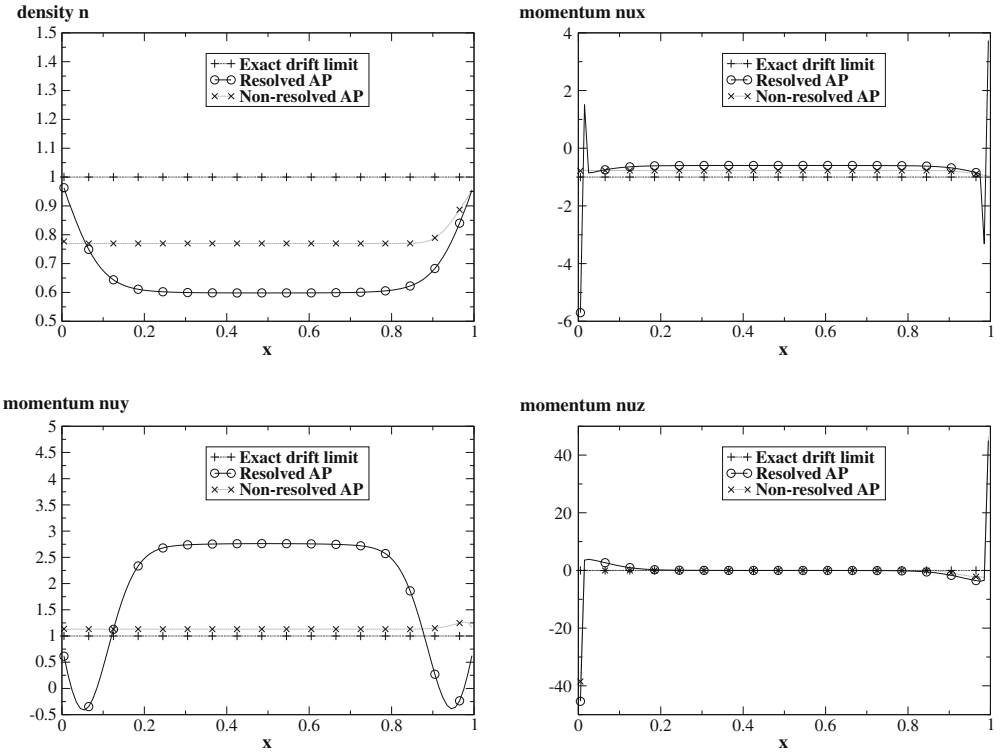

Fig. 10. Comparison of the resolved AP scheme (crosses), and unresolved AP scheme (circles) at $t = 0.1$ for unprepared initial and boundary conditions $\varepsilon = 10^{-6}$ and $\varepsilon' = 10^{-2}$; density n (top left), x-component of the momentum nu_x (top right), y-component of the momentum nu_y (bottom left), z-component of the momentum nu_z (bottom right). The computed solutions are shown for the section at middle $y = 0.5$ of the calculation domain Ω along the x-direction.

well as in the forthcoming pictures, the various physical quantities (i.e. the density n and the three components of the momentum $n\boldsymbol{u}$) are shown as functions of x for a given value of $y = 0.5$. The computed solutions are indistinguishable and very close to the drift-fluid limit.

In this case $\varepsilon \ll 1$, we want to test the consistency of the scheme with the drift-fluid limit. To do so, we compute the difference between the numerical solution and the analytical solution (4.1). This is not the numerical error in the conventional sense, since we do not compare the solution with the exact solution for the same value of ε but rather with the exact solution in the limit $\varepsilon \to 0$. For this reason, we do not call this quantity, 'the error', but rather 'the difference with the drift-fluid limit'. We normalize this difference by the exact value of the drift-fluid limit, except for nu_z since this value is exactly zero. We display these quantities as functions of (x, y) for the resolved AP scheme with the value $\varepsilon = 10^{-6}$ on Fig. 4. The picture is almost the same if we replace the resolved AP scheme by the resolved conventional scheme. For this reason, the latter is omitted.

The maximal relative difference between the computed solution and the exact drift-fluid limit on the density and momenta for three values of ε are given in Table 2 for the resolved conventional scheme and in Table 3 for the resolved AP scheme. They both show a very good agreement with the drift-fluid limit, which increases as ε decreases. This is an expected result since both the resolved conventional and AP schemes use $\Delta t = O(\sqrt{\varepsilon})$. For this range of time-steps the resolved conventional scheme is only slightly more accurate than the resolved AP scheme.

4.2.2. Unresolved case

We now examine the unresolved situation, where $\varepsilon \ll \Delta t$. Results obtained by the non-resolved conventional and AP schemes for $\varepsilon = 10^{-6}$ are displayed in Fig. 5. We recall that "non-resolved" means that the viscosities are computed through (3.32) and the time-step through (3.34) instead of (3.28), (3.31) in the resolved case.

Clearly, the computed solutions with the non-resolved conventional scheme are unstable, while those calculated with the non-resolved AP scheme remain stable and consistent with the exact drift-fluid limit. The difference between the computed solution and the exact drift-fluid limit on the density and momenta (relative difference for n, nu_x and nu_y and absolute difference for nu_z) of the solution for $\varepsilon = 10^{-6}$ are given in Fig. 6 for the non-resolved conventional scheme and in Fig. 7 for the non-resolved AP scheme. They confirm the stability and accuracy of the non-resolved AP scheme and the instability of the non-resolved conventional scheme.

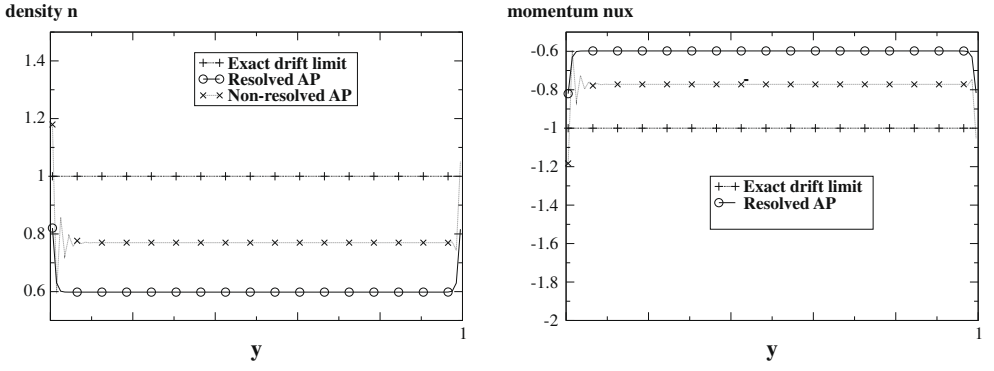

In Table 4, the difference between the computed solution and the exact drift-fluid limit for the non-resolved conventional scheme for the three values of ε are given, and similarly for the non-resolved AP scheme in Table 5. Again, the consistency of the non-resolved AP scheme with the drift-fluid limit on the one hand, and the instability of the non-resolved conventional scheme on the other hand, are confirmed.

Fig. 8, shows the evolution of the time-step with respect to time in the case $\varepsilon = 10^{-6}$ for both the unresolved and resolved AP schemes. We recall that the time-step is not fixed once for all, but is recomputed at each time-step using the CFL condition. However, we can see that, in log scale, the time-step remains about constant. The time-step for the unresolved AP scheme is about 3 decades larger than for the resolved AP scheme. In Table 6, we compare the time-step to the scaled gyro-period and we notice that it is of the same order of magnitude for the resolved AP scheme, as it should, and it is much larger (up to 4 decades!) for the unresolved AP scheme.

It is even more interesting to compare the CPU time between the unresolved AP scheme and the conventional scheme. Indeed, the AP scheme involves more complex computations than the conventional scheme, such as the inversion of linear systems. It is therefore legitimate to wonder whether this additional work does not completely balance the gain obtained through the use of larger time-steps. To check this point, the CPU times for the conventional and non-resolved AP schemes for three values of ε are given in Table 7. We see that the gain in CPU time is up to almost 4 decades with the smallest value of ε. The gain scales about like $\sqrt{\varepsilon}$ as it should.

These comparisons show that the proposed AP schemes are very powerful in handling the numerical approximation of drift-fluid asymptotics.

4.3. Simulations for $\varepsilon = 1$

When $\varepsilon = O(1)$, the resolved and unresolved AP schemes are almost similar and we want to show that they give similar results as the resolved conventional scheme. In this way, we show that the AP scheme is as good as the conventional scheme when $\varepsilon = O(1)$. We have already shown in the previous section that the former is much better than the latter when $\varepsilon \ll 1$.

When $\varepsilon = 1$, the exact solution is no longer the drift-fluid limit solution. So, we restrict ourselves to a comparison between the resolved AP scheme and the resolved conventional scheme. This comparison is shown in Fig. 9. We notice that

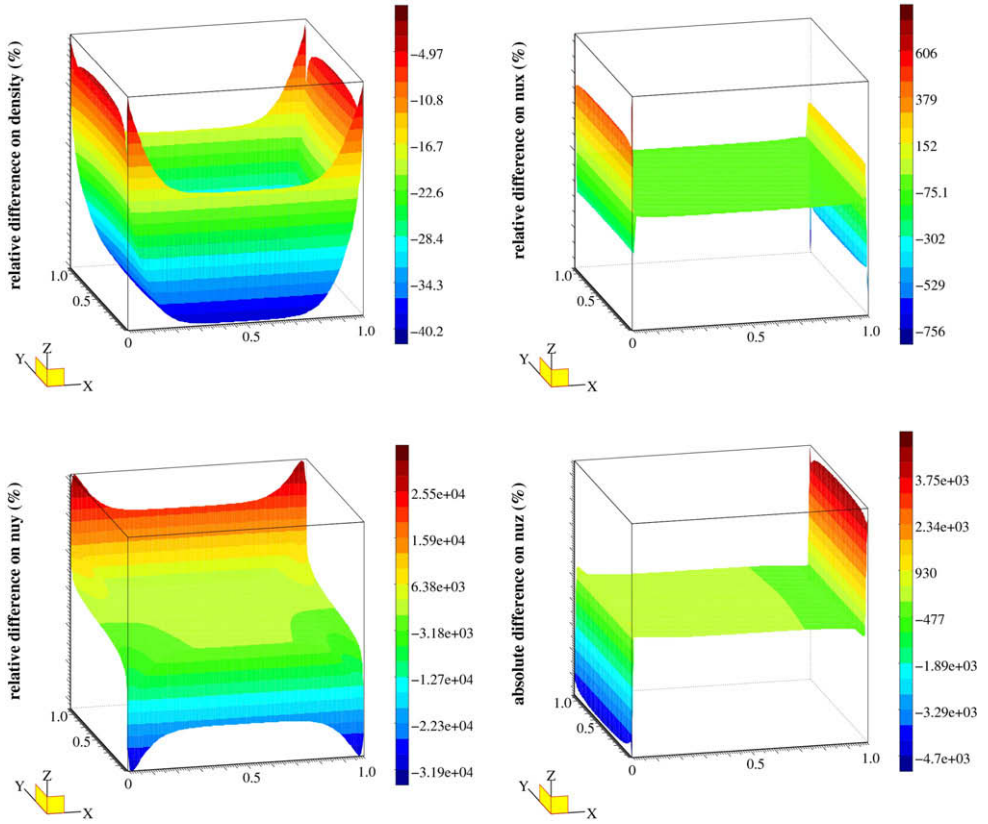

Fig. 12. Relative difference between the computed solution and the exact drift-fluid limit of the resolved AP scheme at time $t = 0.1$ for unprepared initial and boundary conditions $\varepsilon = 10^{-6}$ and $\varepsilon' = 10^{-2}$; density n (top left), x-component of the momentum nu_x (top right), y-component of the momentum nu_y (bottom left). Absolute difference between the computed solution and the exact drift-fluid limit on the z-component of the momentum nu_z (bottom right).

the calculated solutions with the two schemes are indistinguishable. Therefore for ε of order of 1, both the resolved AP scheme and resolved conventional scheme are comparable.

4.4. Simulations for unprepared conditions

For the sake of completeness, we show some numerical results obtained with unprepared boundary conditions. In this context, our guess is that the drift-fluid limit gives the correct behaviour of the solution after a fast initial transient (if the initial conditions are not well-prepared) and far enough from the boundaries where a boundary layer can appear (if the boundary data are not well-prepared). Unfortunately, a rigorous mathematical theory of the drift-fluid limit both in well-prepared and not well-prepared conditions is still lacking and we do not have any proof to support our guess. However, the numerical simulations below show that boundary layers actually appear.

For this purpose, we introduce a second parameter $\varepsilon' = 10^{-2}$ and use initial and boundary conditions as given by Table 1 with ε replaced by ε'. On the other hand, ε is kept at the value $\varepsilon = 10^{-6}$ in the model (2.1), (2.2) and in the scheme (3.1), (3.2).

On Figs. 10 and 11, we display the values of the density and the three components of the momentum as functions of x (resp. y) along the line $y = 0.5$ (resp. $x = 0.5$) for the resolved and non-resolved AP schemes and for the drift-fluid limit. The relative differences (absolute difference in the case of nu_z) of the solution with the drift-fluid limit are given on Fig. 12 for the resolved AP scheme and on Fig. 13 for the non-resolved one.

Both the resolved and non-resolved AP schemes exhibit a significant discrepancy with the drift-fluid limit. This discrepancy originates in the appearance of boundary layers which pollute the accuracy of the solution inside the domain. However, the discrepancy is much larger for the resolved AP scheme than for the non-resolved one. In many instances, the non-resolved AP scheme provides a fairly correct solution and its oscillations inside the boundary layers are less pronounced. This can be attributed to the larger time-steps which provide a stronger relaxation rate towards the drift-fluid limit as well as a bigger amount of numerical diffusion than the small time-steps used in the resolved-AP schemes.

These results show that the use of the non-resolved AP scheme in the case of non well-prepared boundary data at least provides a stable if not accurate solution. Additionally, it is expected that a suitable boundary layer analysis will permit to

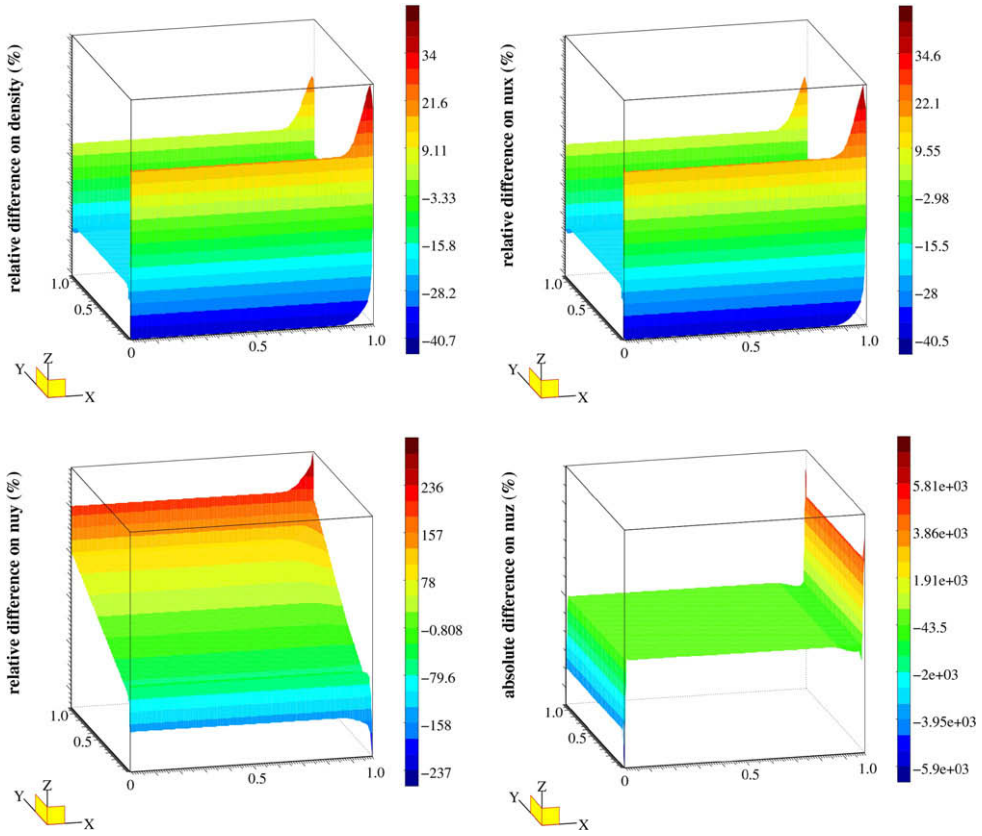

Fig. 13. Relative difference between the computed solution and the exact drift-fluid limit of the non-resolved AP scheme at time $t = 0.1$ for unprepared initial and boundary conditions $\varepsilon = 10^{-6}$ and $\varepsilon' = 10^{-2}$; density n (top left), x-component of the momentum nu_x (top right), y-component of the momentum nu_y (bottom left). Absolute difference between the computed solution and the exact drift-fluid limit on the z-component of the momentum nu_z (bottom right).

derive corrected boundary conditions which will take into account the influence of the boundary layer. The search for adequate boundary layer correctors will be the subject of future work.

5. Conclusion

The Euler–Lorentz model in the drift-fluid scaling for ion flow has been investigated. First the drift-fluid limit has been studied and it has been shown that the parallel fluid velocity to the magnetic field is a solution of an elliptic equation. Then, the full Euler–Lorentz model in the drift-fluid scaling has been investigated. A reformulation of the model has been provided, which shows that the parallel velocity is the solution of a wave equation with wave velocities tending to infinity as the scaling parameter ε goes to zero. This reformulation allows to derive an Asymptotic Preserving scheme for the Euler–Lorentz model in the drift-fluid scaling, i.e. a scheme which is consistent with the full Euler–Lorentz model when $\varepsilon = O(1)$ and which is consistent with its drift-fluid limit when $\varepsilon \to 0$. The scheme allows to compute the solution of the Euler–Lorentz model when $\varepsilon \ll 1$ with a time-step independent of ε. This property has been demonstrated numerically on a test example. It has been shown that the scheme is as good as the conventional scheme when $\varepsilon = O(1)$ and that it provides a stable if not accurate solution in the case of non well-prepared boundary data.

Forthcoming work will be devoted to the application of the AP scheme in the case of time varying and inhomogeneous magnetic fields, the coupling of the ion flow to the electron flow and to the electric and magnetic fields as well as to more rigorous stability analyses of the proposed schemes.

Acknowledgments

The authors wish to express their gratitude to G. Falchetto, X. Garbet and M. Ottaviani from the CEA-Cadarache for fruitful discussions and encouragements. This work has been partially supported by the Marie Curie Actions of the European Commission in the frame of the DEASE project (MEST-CT-2005-021122), by the CNRS and the Association Euratom-CEA in the framework of the contract 'Gyrostab' and by the CEA-Saclay in the framework of the contract 'Astre'# SAV 34160. This work was performed while the third author was a CNRS- Post-Doc at the Institut de Mathématiques de Toulouse.

References

[1] M.A. Beer, S.C. Cowley, G.W. Hammett, Field-aligned coordinates for nonlinear simulations of tokamak turbulence, Phys. Plasmas 2 (1995) 2687.
[2] M.A. Beer, G.W. Hammett, Toroidal gyrofluid equations for simulations of tokamak turbulence, Phys. Plasmas 3 (1996) 4046.
[3] R. Belaouar, N. Crouseilles, P. Degond, E. Sonnendrücker, An asymptotically stable semi-Lagrangian scheme in the quasi-neutral limit, submitted for publication.
[4] C. Buet, S. Cordier, B. Lucquin-Desreux, S. Mancini, Diffusion limit of the Lorentz model: asymptotic preserving schemes, Math. Model. Numer. Anal. 36 (2002) 631.
[5] R. Caflisch, S. Jin, G. Russo, Uniformly accurate schemes for hyperbolic systems with relaxations, SIAM J. Numer. Anal. 34 (1997) 246.
[6] P. Crispel, P. Degond, M-H. Vignal, An asymptotically stable discretization for the Euler–Poisson system in the quasineutral limit, C. R. Acad. Sci. Paris Ser. I 341 (2005) 341.
[7] P. Crispel, P. Degond, M.-H. Vignal, An asymptotic preserving scheme for the two-fluid Euler–Poisson model in the quasineutral limit, J. Comput. Phys. 223 (2007) 208.
[8] P. Degond, F. Deluzet, L. Navoret, An asymptotically stable Particle-in-Cell (PIC) scheme for collisionless plasma simulations near quasineutrality, C. R. Acad. Sci. Paris Ser. I 343 (2006) 613.
[9] P. Degond, S. Jin, J.-G. Liu, Mach-number uniform asymptotic-preserving Gauge schemes for compressible flows, Bull. Inst. Math., Acad. Sinica (New Series) 2 (2007) 851.
[10] P. Degond, S. Jin, M. Tang, On the time splitting spectral method for the complex Ginzburg–Landau equation in the large time and space scale limit, SIAM J. Sci. Comput. 30 (2008) 2466.
[11] P. Degond, J.-G. Liu, M.-H. Vignal, Analysis of an asymptotic preserving scheme for the Euler–Poisson system in the quasineutral limit, SIAM J. Numer. Anal. 46 (2008) 1298.
[12] P. Degond, P.-F. Peyrard, G. Russo, P. Villedieu, Polynomial upwind schemes for hyperbolic systems, C. R. Acad. Sci. Paris Ser. I 328 (1999) 479.
[13] A.M. Dimits, Fluid simulations of tokamak turbulence in quasiballooning coordinates, Phys. Rev. E 48 (1993) 4070.
[14] W. Dorland, G.W. Hammett, Gyrofluid turbulence models with kinetic effects, Phys. Fluids B-Plasmas 5 (1993) 812.
[15] G.L. Falchetto, M. Ottaviani, Effect of collisional zonal-flow damping on flux-driven turbulent transport, Phys. Rev. Lett. 92 (2004) 025002.
[16] X. Garbet, C. Bourdelle, G.T. Hoang, P. Maget, S. Benkadda, P. Beyer, C. Figarella, I. Voitsekovitch, O. Agullo, N. Bian, Global simulations of ion turbulence with magnetic shear reversal, Phys. Plasmas 8 (2001) 2793.
[17] L. Gosse, G. Toscani, Asymptotic preserving and well-balanced schemes for radiative transfer and the Rosseland approximation, Numer. Math. 98 (2004) 223.
[18] L. Gosse, G. Toscani, An asymptotic preserving well-balanced scheme for the hyperbolic heat equation, C. R. Acad. Sci. Paris Ser. I 334 (2002) 337.
[19] K. Hallatschek, A. Zeiler, Nonlocal simulation of the transition from ballooning to ion temperature gradient mode turbulence in the tokamak edge, Phys. Plasmas 7 (2000) 2554.
[20] G.W. Hammett, M.A. Beer, W. Dorland, S.C. Cowley, S.A. Smith, Developments in the gyrofluid approach to tokamak turbulence simulations, Plasma Phys. Contr. Fusion 35 (1993) 973.
[21] R.D. Hazeltine, J.D. Meiss, Plasma Confinement, Dover Publications, Mineola, New York, 2003.
[22] S. Jin, Efficient Asymptotic-Preserving (AP) Schemes for some multiscale kinetic equations, SIAM J. Sci. Comput. 21 (1999) 441.
[23] S. Jin, Runge-Kutta methods for hyperbolic conservation laws with stiff relaxation terms, J. Comput. Phys. 122 (1995) 51.
[24] S. Jin, C.D. Levermore, Numerical schemes for hyperbolic conservation laws with stiff relaxation terms, J. Comput. Phys. 126 (1996) 449.
[25] S. Jin, L. Pareschi, G. Toscani, Diffusive relaxation schemes for discrete-velocity kinetic equations, SIAM J. Numer. Anal. 35 (1998) 2405.
[26] S. Jin, L. Pareschi, G. Toscani, Uniformly accurate diffusive relaxation schemes for multiscale transport equations, SIAM J. Numer. Anal. 38 (2000) 913.
[27] E.M. Lifshitz, L.P. Pitaevskii, Physical Kinetics, Course in Theoretical Physics, vol. 10, Butterworth-Heinemann, Oxford, 2006.

[28] V. Naulin, Electromagnetic transport components and sheared flows in drift-Alfvèn turbulence, Phys. Plasmas 10 (2003) 4016.
[29] V. Naulin, A. Kendl, O.E. Garcia, A.H. Nielsen, J. Juul Rasmussen, Shear flow generation and energetics in electromagnetic turbulence, Phys. Plasmas 12 (2005) 052515.
[30] M. Ottaviani, G. Manfredi, The gyro-radius scaling of ion thermal transport from global numerical simulations of ion temperature gradient driven turbulence, Phys. Plasmas 6 (1999) 3267.
[31] L. Pareschi, G. Russo, Asymptotic preserving Monte Carlo methods for the Boltzmann equation, Transp. Theory Stat. Phys. 29 (2000) 415.
[32] B.D. Scott, Three-dimensional computation of drift Alfvèn turbulence, Plasma Phys. Contr. Fusion 39 (1997) 1635.
[33] B.D. Scott, Free-energy conservation in local gyrofluid models, Phys. Plasmas 12 (2005) 102307.
[34] E.F. Toro, Riemann Solvers and Numerical Methods for Fluids Dynamics, A Practical Introduction, second ed., Springer, Berlin, 1999.
[35] X.Q. Xu, R.H. Cohen, T.D. Rognlien, J.R. Myra, Low-to-high confinement transition simulations in divertor geometry, Phys. Plasmas 7 (2000) 1951.